ACS Sustainable Chemistry & Engineering

Research Article

pubs.acs.org/journal/ascecg

Brilliant IR Reflecting Yellow Colorants in Rare Earth Double Molybdate Substituted $BiVO_4$ Solid Solutions for Energy Saving Applications

S. Sameera, P. Prabhakar Rao,* S. Divya, and Athira K. V. Raj

Materials Science and Technology Division, CSIR–National Institute for Interdisciplinary Science and Technology (NIIST), Thiruvananthapuram 695 019, India

Supporting Information

ABSTRACT: Brilliant IR reflecting yellow colorants are developed in rare earth double molybdate substituted $BiVO_4$ solid solutions. $Li_{0.10}RE_{0.10}Bi_{0.8}Mo_{0.2}V_{0.8}O_4$ (RE = La, Pr, Sm, Gd, Tb, Dy, Y, Yb and Lu) pigments are prepared by a conventional solid-state reaction route and their optical, structural and morphological properties are analyzed. X-ray diffraction analysis confirms the tetragonal scheelite phase formation in the series. These pigments have a strong optical absorption in the UV-blue light wavelength region. CIE LAB color analysis shows that different hues of yellow shades are obtained in these solid solutions. The color characteristics are comparable to commercial $BiVO_4$ pigment. Incorporation of double rare earth molybdates of La, Gd, Tb, Y and Lu into $BiVO_4$ results in nontoxic IR reflecting cool pigments. The applicability of the developed pigment was tested on a concrete cement surface as well as on a metal panel. These pigments are composed of less toxic elements that make them favorable for energy saving surface coating formulations for buildings and automotives.

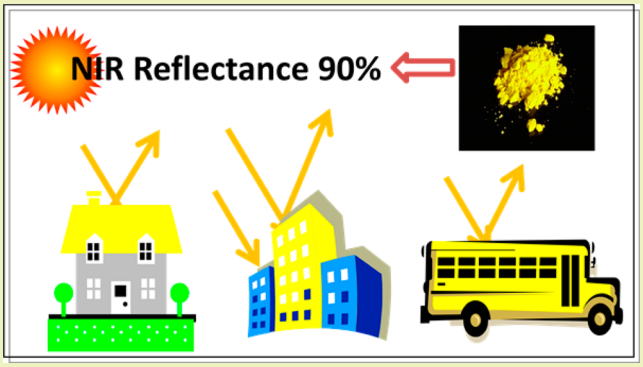

KEYWORDS: *Bismuth vanadate, Lithium rare earth double molybdates, Tetragonal scheelite, Yellow pigments, Less toxic elements, Infrared reflectance*

INTRODUCTION

The urban heat island effect emerging in metropolitan cities produces elevated urban air temperatures. Solar radiation consists of about 5% ultraviolet radiation, 46% visible radiation and 49% infrared radiation. A major contribution of heat comes from the IR radiation, which transfers heat to the underlying structure in buildings and automotives causing thermal discomfort and health problems. A substantial amount of energy is consumed to cool buildings, thus increasing energy demand.[1] Cool paints absorb less solar energy, which keeps the surface at a lower temperature and decreases energy transfer by radiation. Passive cooling of buildings helps reduction in air pollution due to low energy usage and power plant emissions. Therefore, current interest in the pigment industry is focused on developing nontoxic cool pigments that aid in energy savings.[2] Bright yellow shades are particularly challenging, with preferential reformulation away from cadmium pigments and lead chromates within the plastics and surface coating markets.[3] There is an urgent need for developing IR reflecting nontoxic yellows, which are limited in the current market.

Recently, $BiVO_4$ has attracted wide attention for its photocatalytic,[4] ferroelastic,[5] dielectric,[6] ionic and electronic conductive properties,[7] which makes it attractive for use in gas sensors,[8] microwave resonator devices,[6] wastewater treatment[9] and water splitting.[9] $BiVO_4$ has been identified as an ideal candidate for pigmentary applications.[10] Recently, many researchers, including our group, have reported $BiVO_4$ based pigments such as (Bi, La)VO_4,[11] (Bi, Ca, Zn)VO_4,[12] (Bi, Ca, Zn, La)VO_4,[13] Y and Nb doped $BiVO_4$[14] and SiO_2 coated $BiVO_4$.[15] So, development of nontoxic IR reflecting $BiVO_4$ based pigments can lead to cool surface coating formulations for buildings and automobile shells.

Double alkali rare earth molybdates and tungstates of the type $ARE(XO_4)_2$; X = Mo, W[16] have a variety of applications in optoelectronics,[17] catalysis and so on. Mostly depending on the relation between ionic radii of A and RE, they crystallize in diverse symmetries: tetragonal, orthorhombic, monoclinic and even triclinic.[18] They crystallize in various structural forms according to the ratio of R_{RE}/R_A. Among the alkali metals, we have chosen lithium rare earth molybdates to form solid solutions with $BiVO_4$ to further ameliorate its color parameters. $BiVO_4$ has three main crystal forms: zircon structure with tetragonal system[19] and scheelite structure with monoclinic[20] and tetragonal systems.[7] $BiVO_4$ undergoes a reversible second

Received: March 13, 2015
Revised: May 2, 2015
Published: May 13, 2015

DOI: 10.1021/acssuschemeng.5b00198
ACS Sustainable Chem. Eng. 2015, 3, 1227–1233

order ferroelastic phase transition from monoclinic scheelite to tetragonal scheelite, which can be induced by a high temperature of about 255 °C or high pressure.[21] This phase transition can also be achieved by incorporating larger ions than V^{5+} at the B-site, as shown in our recent research.[14] We have reported the effect of $(LiLa)_{1/2}MoO_4$ substitution on $BiVO_4$, leading to $[(Li_{0.5}La_{0.5})_xBi_{1-x}][Mo_xV_{1-x}]O_4$ based pigments.[22] $Li_{0.10}La_{0.10}Bi_{0.8}Mo_{0.2}V_{0.8}O_4$ composition exhibited intense yellow color characterized by the highest b^* value among the developed pigments. Rare earths show interesting optical properties, as they have a partially filled f orbital. Thus, rare earth substitution allows further tuning of band gap of the material. In this regard, we made an attempt to substitute various rare earths in the selected composition to produce various colorants. $Li_{0.10}RE_{0.10}Bi_{0.8}Mo_{0.2}V_{0.8}O_4$; RE = La, Pr, Sm, Gd, Tb, Dy, Y, Yb and Lu pigments were prepared and analyzed for their crystalline structure, morphological, composition and optical characteristics. The relationship between observed band gap and the color characteristics of these materials has been emphasized. Their perspectives for application as IR reflecting cool pigments have been evaluated by coating on various substrates like concrete cement and metal panel.

EXPERIMENTAL SECTION

General and Synthesis. The pigments of the formula $Li_{0.10}RE_{0.10}Bi_{0.8}Mo_{0.2}V_{0.8}O_4$ were prepared by the conventional solid state reaction route. Li_2CO_3 (99.9% purity, Acros Organics), La_2O_3, Pr_6O_{11}, Sm_2O_3, Gd_2O_3, Tb_4O_7, Dy_2O_3, Y_2O_3, Yb_2O_3, Lu_2O_3, V_2O_5 (99.99% purity, Sigma-Aldrich), Bi_2O_3 (99.999% purity, Sigma-Aldrich) and MoO_3 (99.5% purity, Sigma-Aldrich) were weighed in the required stoichiometric amount and then were wet mixed thoroughly in an agate mortar using acetone as the medium. For comparison, $BiVO_4$ samples were also prepared. The mixed product was dried in an air oven at 100 °C for 1 h. The process of mixing and drying was repeated three times to get a homogeneous mixture. The dried mixture was then calcined in a platinum crucible in an electrical furnace. The heating of the furnace was programmed increasing the temperature initially at 10 °C per minute up to the temperature (400–500 °C) and afterward, the heating rate was decreased to 5 °C per minute up to the required temperature (800 °C). The samples were soaked at the final temperature 800 °C for 6 h. The calcined samples were ground thoroughly in an agate mortar into fine powder.

Characterizations. The calcined powders were characterized by means of X-ray powder diffraction (XRD) using a Ni filtered Cu Kα radiation with a PANalytical X'pert Pro diffractometer operated at 45 kV and 30 mA for its crystalline structure. Data were collected from 10 to 90° 2θ range with a step size of 0.016°. Particle morphological analysis of the powder was performed by means of scanning electron microscopy (SEM) with a JEOL JSM-5600 LV SEM instrument with an acceleration voltage of 15 kV. Energy dispersive X-ray spectroscopy (EDS) analysis and elemental mapping of the samples were analyzed using silicon drift detector X-MaxN attached with a Carl Zeiss EVO SEM apparatus. EDS elemental mapping was conducted by AZtec Energy EDS Microanalysis software. The UV visible spectra of the samples was measured with a UV–vis-NIR spectrophotometer (Shimadzu, UV-3600) using $BaSO_4$ as a reference. Optical measurements were performed in the 220 to 800 nm wavelength range with a step size of 2 nm. The measurement conditions were as follows: an illuminant D65, 10° complementary observer and measuring geometry d/8°. The color coordinates were determined by coupling analytical software (UVPC Color Analysis Personal Spectroscopy Software V3, Shimadzu) to the UV-3600 spectrophotometer. The color of the pigments was evaluated according to The Commission Internationale del' Eclairage (CIE) through $L^*a^*b^*$ 1976 color scales (CIE-LAB 1976 color scales). In this system L^* is the color lightness (L^* is zero for black and 100 for white), a^* is the green (−)/ red (+) axis, and b^* is the blue (−)/yellow (+) axis. The parameter C^* (chroma) represents saturation of the color and $h°$ represents the hue angle. The chroma is defined as $C^* = ((a^*)^2 + (b^*)^2)^{1/2}$. The hue angle, $h°$ is expressed in degrees and ranges from 0° to 360° and is calculated using the formula $h° = \tan^{-1}(b^*/a^*)$. The infrared reflectance of the powdered pigment samples was measured with a UV–vis-NIR spectrophotometer (Shimadzu, UV-3600 with an integrating sphere attachment) using polytetrafluoroethylene (PTFE) as a reference in the 700 to 2500 nm range with a step size of 5 nm. The IR solar reflectance in the wavelength range from 700 to 2500 nm was calculated in accordance with the ASTM standard number G173-03.[23] The IR solar reflectance is expressed as the integral of the percent reflectance times the solar irradiance divided by the integral of the solar irradiance when integrated over the 700–2500 nm range as shown in the formula,

$$R = \frac{\int_{700}^{2500} r(\lambda) i(\lambda) d\lambda}{\int_{700}^{2500} i(\lambda) d\lambda}$$

where $r(\lambda)$ is the spectral reflectance obtained from the experiment and $i(\lambda)$ is the standard solar spectrum (Wm^{-2} nm^{-1}) obtained from the standard.

RESULTS AND DISCUSSION

Figure 1a shows the powder X-ray diffraction patterns of pigments calcined at 800 °C. XRD analysis indicates that the pigments are highly crystalline in nature. All the reflections are indexed as per the monoclinic tetragonal (s-t) phase with a space group $I4_{1/a}$ and the reflections can be well indexed

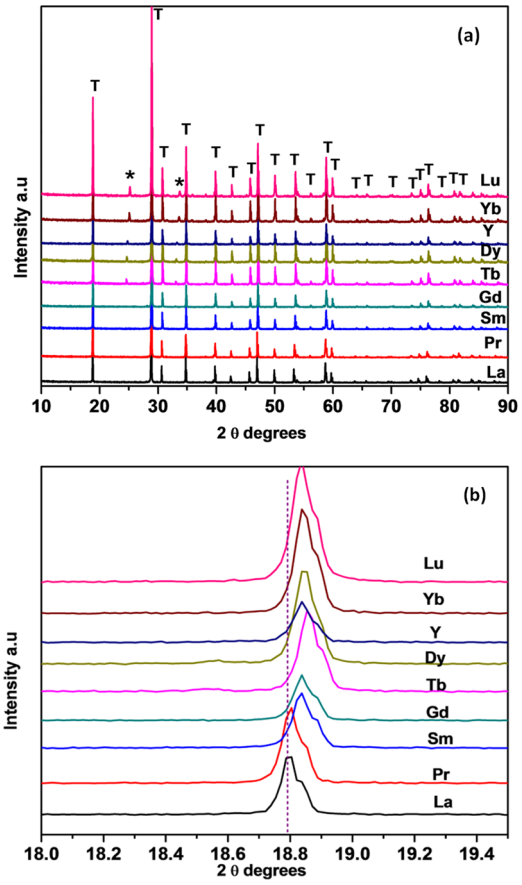

Figure 1. (a) X-ray powder diffraction patterns of $Li_{0.10}RE_{0.10}Bi_{0.8}Mo_{0.2}V_{0.8}O_4$ pigments; (b) Zoomed view of peak position around 18.8°.

DOI: 10.1021/acssuschemeng.5b00198
ACS Sustainable Chem. Eng. 2015, 3, 1227–1233

according to the powder diffraction file no. 01-074-4892. Figure 1b shows the zoom-in part of the range of 2θ from 18−19.5°. The line in Figure 1b indicates the inclination of the shift of the (101) peak toward the higher angle side as the decrease of ionic radius of rare earth. From Tb onward, minor $REVO_4$ phase formation starts to occur with evidence of peaks around 24° and 33° trending toward higher angles with heavier rare earths.

The structural refinement of all the XRD patterns for rare earth doped $Li_{0.10}RE_{0.10}Bi_{0.8}Mo_{0.2}V_{0.8}O_4$ pigments were performed by the Rietveld analysis using the X'Pert Plus program. The starting model for the refinement of the phases was taken from the reported crystal structure of $BiVO_4$. Here Bi/Li/RE are at (4*b*: 0, 1/4, 5/8) sites, V and Mo at (4*a*: 0, 1/4, 1/8) sites and O at (16*f*: *x*, *y*, *z*), $z = 4$ in the space group $I4_{1/a}$, no. 88. The profile was fitted using a Pseudo Voigt profile function and Caglioti profile parameters were refined. Figure S1 of the Supporting Information shows the typical best fit for sample $Li_{0.10}Gd_{0.10}Bi_{0.8}Mo_{0.2}V_{0.8}O_4$ with the observed, calculated, the difference powder diffraction profiles and the expected Bragg reflections. The refined lattice parameters obtained from the Rietveld analysis of the powder diffraction data for the samples are given in Table S1 of the Supporting Information. As said earlier, space group $I4_{1/a}$ is observed for R_{RE}/R_A over the range from 1.341 to 0.805 for alkali rare earth double molybdates. Here too the obtained solid solutions exhibit the values within this range.

Figure 2 shows the reflectance spectra of $Li_{0.10}RE_{0.10}Bi_{0.8}Mo_{0.2}V_{0.8}O_4$ pigments. UV Visible spectra

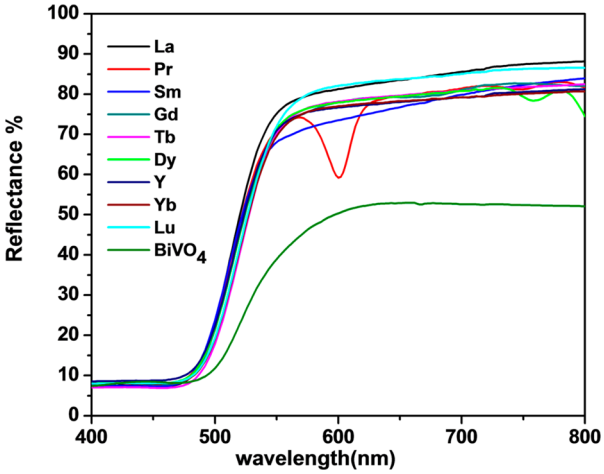

Figure 2. Reflectance spectra of $Li_{0.10}RE_{0.10}Bi_{0.8}Mo_{0.2}V_{0.8}O_4$ pigments.

exhibit shift in absorption edge with respect to different rare earths. Visible light absorption in $BiVO_4$ is due to the excitation of electrons from VB consisting of Bi 6s and O 2p to CB of V 3d orbitals of VO_4^{3-}. As a crystalline semiconductor, the optical absorption near the band edge observes the formula[24]

$$\alpha h\nu = A(h\nu - \mathrm{Eg})^{n/2} \quad (1)$$

where α, ν, Eg and A are absorption coefficient, light frequency, band gap and a constant, respectively. Among them, n depends on the characteristics of the transition in a semiconductor, i.e., direct transition ($n = 1$) or indirect transition ($n = 4$). For $BiVO_4$, the value of n is 1.[25] The band gap energy (Eg value) of $BiVO_4$ can thus be calculated from a Tauc plot, which is $(\alpha h\nu)^2$ versus photon energy ($h\nu$). The intercept of the tangent to the *x*-axis will give a good estimation of the band gap energy for the pigments. The band gap energy for the pigments are given in Table1. There is an increase of band gap compared to $BiVO_4$.

Table 1. CIE Color Coordinates and Band Gap of $Li_{0.10}RE_{0.10}Bi_{0.8}Mo_{0.2}V_{0.8}O_4$ Pigments

RE	*L**	*a**	*b**	*C**	h^0	Eg (eV)
La	83.30	6.04	81.86	82.08	85.77	2.50
Pr	80.39	2.08	75.50	75.53	88.41	2.48
Sm	80.47	4.63	77.06	77.19	86.55	2.45
Gd	81.44	5.51	79.94	80.13	86.05	2.43
Tb	80.70	9.99	80.35	80.97	82.90	2.46
Dy	81.33	−3.15	77.88	77.95	92.33	2.45
Y	81.57	7.26	77.34	77.68	84.63	2.44
Yb	80.59	9.13	76.49	77.04	83.18	2.45
Lu	82.05	10.8	78.72	79.46	82.18	2.46
$BiVO_4$	65.79	14.29	52.57	54.47	74.78	2.37
sicopal yellow[12]	94.40	−16.7	76.9	78.7	77.8	2.51

This means that the empty 3d orbital of V^{5+} in solid solution is incorporated by extra energy levels. With the incorporation of alkali rare earth double molybdates, there is a shift of spectra toward shorter wavelength. The optical band gap variation of rare earth sesquioxides has been studied by Prokofiev et al., who has stated that the occupied 4f band in rare earth sesquioxides lies above the O 2p level, and hence the 4f-d transition determines band gap.[26] In the case of La, there is absence of f electrons and the inclusion of Mo 4d and La 5d orbitals above the V 3d orbitals results in widening of conduction band. This leads to reduced interaction between O 2p and V 3d orbitals. It might be suggested that such partial occupation of V 3d orbital is originated from the hybridization among Mo 4d, La 5d and V 3d orbitals. This in turn increases the band gap to 2.51 eV. The variation of Eg can be explained by the energy of the RE 4f levels lowering in energy with an increasing occupation of 4f electrons. The occupied 4f band in Pr oxide lies above the O 2p band, and thus, 4f-5d transition may determine the band gap energy. The 4f electronic level gradually becomes lowered with an increase of their atomic number, finally lying in the valence band, which results in an increase of band gap energy from Pr to Sm. The high stability of the half- and fully filled 4f shells causes the position of the 4f orbital of Gd and Lu oxides to locate deep in the valence band causing the high band gap values. As soon as the f-band enters into the 2p band, the Eg values gradually increase. The presence of Y 4d level changes the band structure by modifying the conduction band with Mo 4d above the V 3d orbital and the band gap calculated is 2.44 eV. Figure 3 shows the schematic representation of the band structures of $BiVO_4$ and $Li_{0.10}RE_{0.10}Bi_{0.8}Mo_{0.2}V_{0.8}O_4$ pigments. Zhou et al. studied the role of rare earths in Bi_2RNbO_7 where the position of the 4f band of the rare earth ion in Bi_2RNbO_7 determined the band gap.[27] The importance of partially filled 4f shell in layered perovskite tantalates has been reported by Machida et al.[28] Considering the presence of zircon type rare earth vanadates, from Tb onward, a slight modification in band structure is expected. The zircon structure and tetragonal crystal structure consist of isolated VO_4 tetrahedra and AO_8 dodecahedra. A study by Panchal et al. reveals that most of the features of the band structure in scheelite are qualitatively similar to the ones in the zircon structure.[29] This difference in RE 4f levels and the

DOI: 10.1021/acssuschemeng.5b00198
ACS Sustainable Chem. Eng. 2015, 3, 1227−1233

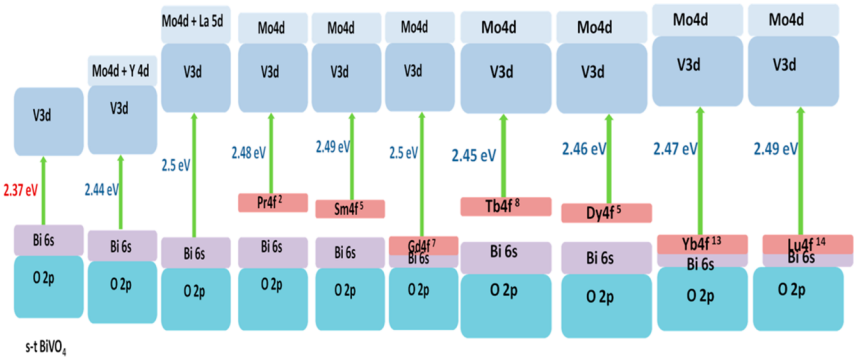

Figure 3. Schematic band structure diagrams of $BiVO_4$ and $Li_{0.10}RE_{0.10}Bi_{0.8}Mo_{0.2}V_{0.8}O_4$ pigments.

corresponding difference in the band gaps lead to different colors.

Table 2 displays the CIE 1976 color coordinates of the $Li_{0.10}RE_{0.10}Bi_{0.8}Mo_{0.2}V_{0.8}O_4$ pigments. Incorporation of various

Table 2. IR Solar Reflectance and Color Coordinates of $Li_{0.10}RE_{0.10}Bi_{0.8}Mo_{0.2}V_{0.8}O_4$ Pigments; RE = La, Gd Coated over Concrete Cement Surface and Metal Panel

parameter	La (concrete)	Gd (concrete)	La (metal)	Gd (metal)
L^*	86.24	87.73	79.63	79.37
a^*	3.22	3.79	−2.33	−1.98
b^*	90.98	86.87	83.71	76.28
C^*	91.04	86.95	83.75	76.3
h^0	87.98	87.50	91.61	91.49
IR R (%)	90	87	70	69
IR R^*(%)	89	86	71	67

alkali rare earth double molybdates into $BiVO_4$ enhances the yellow component (b^* from 52.57 to 81.86). The chroma (C^*) range from 75.53 to 82.08 and hue angle (h^0) values from 82.18 to 92.33. The hue angles ($h°$) of the samples imply the intense yellow color of the developed pigments ($h° = 70–105°$ for yellow). Figure 4 presents the comparison of color coordinates (C^*) and ($h°$) of samples indicating the enhancement in yellow hue comparable to commercial sicopal yellow L 1100[13] as well as molybdenum doped cerium gadolinium oxide.[30] The absorption edge varies with various RE accompanying with the changes of the width or the position of the valence bands

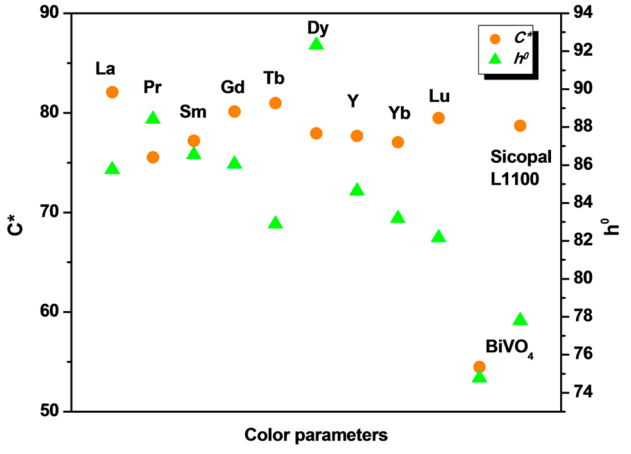

Figure 4. CIE LAB 1976 color coordinates (C^*) and (h^*) of $Li_{0.10}RE_{0.10}Bi_{0.8}Mo_{0.2}V_{0.8}O_4$ pigments with different rare earths.

and conduction bands, which may be one of the reasons for the widening of the optical gap. As a result, the chromaticity of the pigments depends on the identity of the rare earth element. La incorporation gives the highest b^* value of 81.86.

The SEM micrographs obtained are shown in Figure 5. The particles are agglomerated, to some extent. SEM analysis shows that the morphology is irregular and the average size of sample is about 4–7 μm. Compared to $BiVO_4$, there is a marked difference in particle size. There is a slight variation in particle size upon rare earth variation. The EDS was used to further determinate the chemical composition of the as-obtained pigments. The EDS spectrum (Figure S3 of the Supporting Information) of the $Li_{0.10}Gd_{0.10}Bi_{0.8}Mo_{0.2}V_{0.8}O_4$ sample shows the presence of Bi, V, Gd, Mo and O elements, with close approximation to the calculated value. The Li element is not detected due to going beyond the detection range of the instrument. X-ray mapping analysis also reveals that the elements are uniformly distributed within the matrix. The results confirm solid solution formation between $(LiRE)_{1/2}MoO_4$ and $BiVO_4$, leading to a $Li_{0.10}RE_{0.10}Bi_{0.8}Mo_{0.2}V_{0.8}O_4$ pigments system, agreeing with the XRD analysis above. SEM EDS analysis confirms the close agreement between the stoichiometric and the actual composition.

The IR reflectance spectra of selected pigments are displayed in Figure 6. IR reflectance follows the order La > Lu > Gd > Pr > Tb > Y > Yb > Sm > Dy in the 1100 nm range. Certain transitions in NIR region is observed for Pr, Sm, Dy and Yb. Therefore, these rare earths are not favorable for use as IR reflecting colorants. The highest IR reflectance of 90% was observed for La based pigment.

Application Study. To analyze the suitability of the developed pigments for cool roof applications, their performance was tested on a building roofing material, concrete cement. The particular pigments $Li_{0.10}La_{0.10}Bi_{0.8}Mo_{0.2}V_{0.8}O_4$ and $Li_{0.10}Gd_{0.10}Bi_{0.8}Mo_{0.2}V_{0.8}O_4$ were selected to prepare IR reflecting coatings. The coating was done in a two-step process. In the first step, the concrete cement block is precoated with TiO_2, an inexpensive white pigment possessing high IR reflectance. In the second step, the designed typical pigment is applied to the precoated substrate material. The pigment samples were ground and was ultrasonicated (Vibronics, 250W, India) for 10 min to ensure the complete dispersion of the pigment particles in acrylic acid using polyurethane as a binder. The resulted viscous solution was coated on the concrete sheet surface and was allowed to dry in an oven at 150 °C. The thickness of the paint films was estimated using Bruker's DektakXT stylus profiler. The thickness of the films was in 40–45 μm range.

DOI: 10.1021/acssuschemeng.5b00198
ACS Sustainable Chem. Eng. 2015, 3, 1227–1233

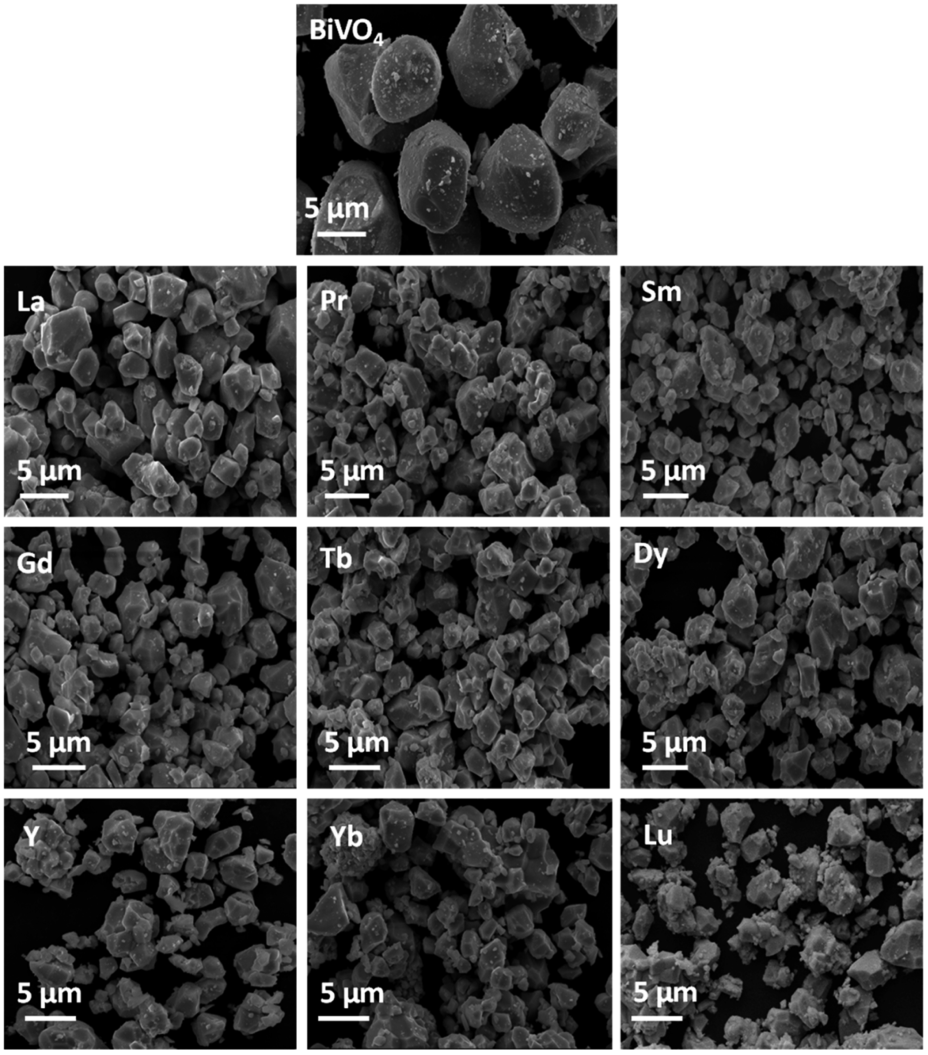

Figure 5. SEM micrographs of $Li_{0.10}RE_{0.10}Bi_{0.8}Mo_{0.2}V_{0.8}O_4$ pigments.

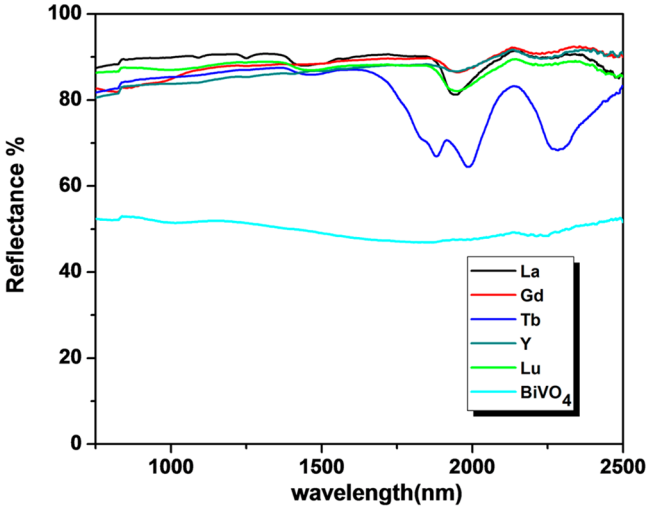

Figure 6. IR Reflectance spectra of $Li_{0.10}RE_{0.10}$ $Bi_{0.8}Mo_{0.2}V_{0.8}O_4$ pigments with selected rare earths; RE = La, Gd, Tb, Y and Lu.

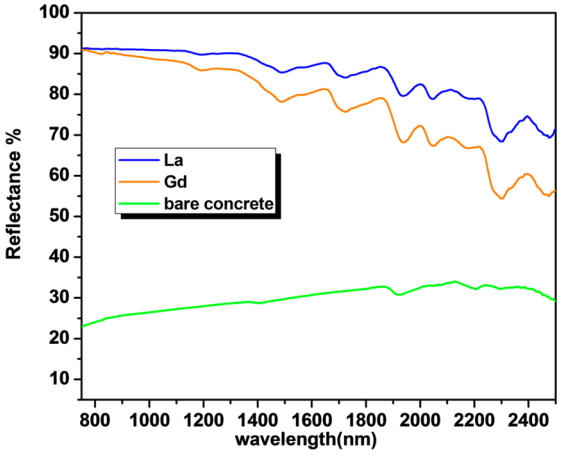

Figure 7. IR reflectance spectra of $Li_{0.10}RE_{0.10}Bi_{0.8}Mo_{0.2}V_{0.8}O_4$; RE = La, Gd pigments coated over concrete cement surface.

The IR reflectance spectrum of the pigments coated over bare concrete cement surface is shown in Figure 7. The IR solar reflectance spectra determined in accordance with ASTM standard G173-03[23] is shown in Figure 8, and the photographs of the resultant coating samples are shown in the inset. The results clearly indicate that a bare concrete surface possesses a low IR reflectance of 27% and IR solar reflectance of 25%. The results point out that these coatings can enhance the IR solar reflectance. The color coordinates of these coatings were

DOI: 10.1021/acssuschemeng.5b00198
ACS Sustainable Chem. Eng. 2015, 3, 1227−1233

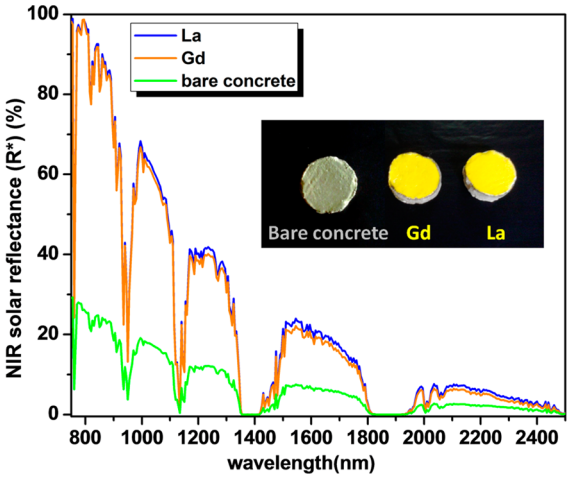

Figure 8. IR solar reflectance spectra of $Li_{0.10}RE_{0.10}$ $Bi_{0.8}Mo_{0.2}V_{0.8}O_4$ pigments; RE = La, Gd coated over concrete cement surface (inset: photographs of samples).

determined using a portable spectrophotometer Miniscan EZ 4000S (Hunter Lab USA) (Table 2). These nonwhite coatings can reduce the surface temperature of the roof and lead to energy savings.

Conventional colored coatings used in automotives increase the interior temperatures. This leads to increased air conditioning usage, which affects the fuel consumption of the vehicle. The performance of particular pigments $Li_{0.10}La_{0.10}Bi_{0.8}Mo_{0.2}V_{0.8}O_4$ and $Li_{0.10}Gd_{0.10}Bi_{0.8}Mo_{0.2}V_{0.8}O_4$ was tested on an aluminum metal sheet to evaluate their applicability in automobiles. The coating procedure was done in a single step procedure where TiO_2 was not used as base coat. The IR solar reflectance values obtained for $Li_{0.10}La_{0.10}Bi_{0.8}Mo_{0.2}V_{0.8}O_4$ and $Li_{0.10}Gd_{0.10}Bi_{0.8}Mo_{0.2}V_{0.8}O_4$ were 71 and 67, respectively. The IR reflectance of the coatings over metal sheets is illustrated in Figure 9. The IR solar reflectance spectra determined in accordance with ASTM standard G173-03[23] of the same is shown in Figure 10, and the photographs of the resultant coating samples are shown in the inset. The results point out that these coatings can enhance the IR solar reflectance. The color coordinates of these coatings are shown in Table 2. The color values indicate enhanced

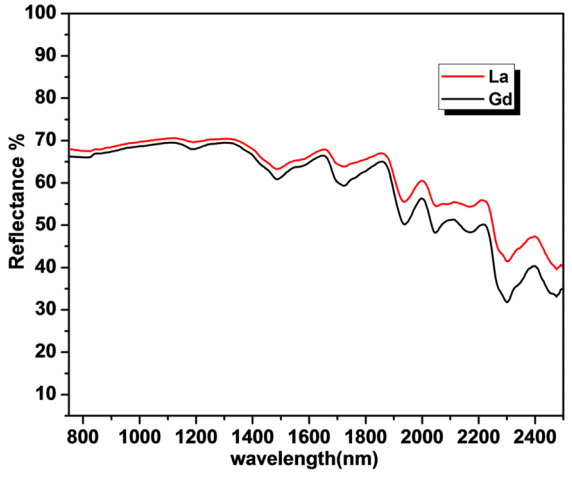

Figure 9. IR reflectance spectra of $Li_{0.10}RE_{0.10}Bi_{0.8}Mo_{0.2}V_{0.8}O_4$; RE = La, Gd pigments coated over a metal panel.

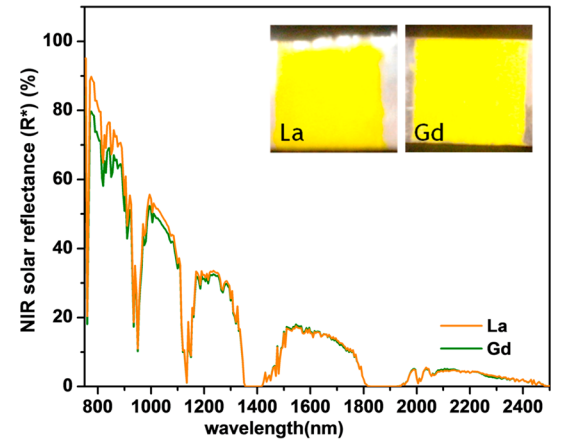

Figure 10. IR solar reflectance spectra of $Li_{0.10}RE_{0.10}$ $Bi_{0.8}Mo_{0.2}V_{0.8}O_4$ pigments; RE = La, Gd coated over a metal panel (inset: photographs of samples).

coloration to the concrete and metal substrate. These cool light colored coatings can thus reduce the energy consumption required for cooling the interior of automobiles and buildings.

CONCLUSIONS

New ecological yellow pigments have been successfully prepared via a solid-state route by effective solid solution formation between $BiVO_4$ and various rare earths in $(LiRE)_{1/2}MoO_4$, leading to $Li_{0.10}RE_{0.10}Bi_{0.8}Mo_{0.2}V_{0.8}O_4$ pigments. Interesting hues of yellow shades were obtained using different rare earths. Remarkable IR reflectance was observed for La, Lu, Gd, Tb and Y in $Li_{0.10}RE_{0.10}Bi_{0.8}Mo_{0.2}V_{0.8}O_4$ pigments. The developed pigments could confer their color as well as IR reflecting properties to the substrate studied. These pigments, as cool coatings, can lead to the sustainability of roofs. Also, their use in automotives will lead to energy saving coatings.

ASSOCIATED CONTENT

Supporting Information

Structural data obtained from Reitveld analysis; XRD pattern fit of $Li_{0.10}Gd_{0.10}Bi_{0.8}Mo_{0.2}V_{0.8}O_4$ after Rietveld refinement; chemical compositions determined by EDS analysis and X-ray dot mapping of $Li_{0.10}Gd_{0.10}Bi_{0.8}Mo_{0.2}V_{0.8}O_4$ pigment. The Supporting Information is available free of charge on the ACS Publications website at DOI: 10.1021/acssuschemeng.5b00198.

AUTHOR INFORMATION

Corresponding Author

*P. P. Rao. E-mail: padala_rao@yahoo.com. Tel.: + 91 471 2515311.

Notes

The authors declare no competing financial interest.

ACKNOWLEDGMENTS

The authors acknowledge financial support from the Council of Scientific and Industrial Research (CSIR NetWork Project SURE CSC0132), New Delhi. One of the authors, Sameera S. also acknowledges Council of Scientific and Industrial Research (CSIR), Government of India, for the financial support toward a Senior Research Fellowship.

DOI: 10.1021/acssuschemeng.5b00198
ACS Sustainable Chem. Eng. 2015, 3, 1227−1233

ABBREVIATIONS

CIELAB = Commission Internationale del' Eclairage 1976
IR = Infrared

REFERENCES

(1) Santamouris, M.; Synnefa, A.; Karlessi, T. Using advanced cool materials in the urban built environment to mitigate heat islands and improve thermal comfort conditions. *Sol. Energy* **2011**, *85* (12), 3085−3102.

(2) Levinson, R.; Berdahl, P.; Akbari, H. Solar spectral optical properties of pigments—Part II: Survey of common colorants. *Sol. Energy Mater. Sol. Cells* **2005**, *89* (4), 351−389.

(3) Hempelmann, U.; Buxbaum, G.; Völz, H. G. Introduction. In *Industrial Inorganic Pigments* [Online]; Buxbaum, G.; Pfaff, G., Eds.; WILEY-VCH Verlag GmbH & Co KGaA: Weinheim, 2005; pp 9−10.

(4) Kudo, A.; Ueda, K.; Kato, H.; Mikami, I. Photocatalytic O_2 evolution under visible light irradiation on $BiVO_4$ in aqueous $AgNO_3$ solution. *Catal. Lett.* **1998**, *53* (3−4), 229−230.

(5) Manolikas, C.; Amelinckx, S. Ferroelastic domains in $BiVO_4$. *Phys. Status Solidi A* **1980**, *60* (1), 167−172.

(6) Valant, M.; Suvorov, D. Chemical compatibility between silver electrodes and low-firing binary-oxide compounds: Conceptual study. *J. Am. Ceram. Soc.* **2000**, *83* (11), 2721−2729.

(7) Hoffart, L.; Heider, U.; Huggins, R. A.; Witschel, W.; Jooss, R.; Lentz, A. Crystal growth and conductivity investigations on $BiVO_4$ single crystals. *Ionics* **1996**, *2* (1), 34−38.

(8) Sun, Y.; Wu, C.; Long, R.; Cui, Y.; Zhang, S.; Xie, Y. Synthetic loosely packed monoclinic $BiVO_4$ nanoellipsoids with novel multi-responses to visible light, trace gas and temperature. *Chem. Commun.* **2009**, *30*, 4542−4544.

(9) Xi, G.; Ye, J. Synthesis of bismuth vanadate nanoplates with exposed {001} facets and enhanced visible-light photocatalytic properties. *Chem. Commun.* **2010**, *46* (11), 1893−1895.

(10) Endriss, H. Bismuth vanadates. In *High Performance Pigments*; Wiley-VCH Verlag GmbH & Co. KGaA: Weinheim, 2009; pp 7−12.

(11) Wendusu; Ikawa, K.-i.; Masui, T.; Imanaka, N. Novel environment-friendly yellow pigments based on (Bi, La)VO_4. *Chem. Lett.* **2011**, *40* (8), 792−794.

(12) Masui, T.; Honda, T.; Wendusu; Imanaka, N. Novel and environmentally friendly (Bi,Ca,Zn)VO_4 yellow pigments. *Dyes Pigm.* **2013**, *99* (3), 636−641.

(13) Wendusu; Honda, T.; Masui, T.; Imanaka, N. Novel environmentally friendly (Bi, Ca, Zn, La)VO_4 inorganic yellow pigments. *RSC Adv.* **2013**, *3* (47), 24941−24945.

(14) Sameera, S. F.; Rao, P. P.; Kumari, L. S.; James, V.; Divya, S. Potential NIR reflecting yellow pigments in $(BiV)_{1-x}(YNb)_xO_4$ solid solutions. *Chem. Lett.* **2013**, *42* (5), 521−523.

(15) Strobel, R.; Metz, H. J.; Pratsinis, S. E. Brilliant yellow, transparent pure, and SiO_2-coated $BiVO_4$ nanoparticles made in flames. *Chem. Mater.* **2008**, *20* (20), 6346−6351.

(16) Maier, A. A.; Provotorov, M. V.; Balashov, V. A. Double molybdates and tungstates of the rare earth and alkali metals. *Russ. Chem. Rev.* **1973**, *42* (10), 822.

(17) Kato, A.; Oishi, S.; Shishido, T.; Yamazaki, M.; Iida, S. Evaluation of stoichiometric rare-earth molybdate and tungstate compounds as laser materials. *J. Phys. Chem. Solids* **2005**, *66* (11), 2079−2081.

(18) Chimitova, O. D.; Atuchin, V. V.; Bazarov, B. G.; Molokeev, M. S.; Bazarova, Z. G. The formation and structural parameters of new double molybdates $RbLn(MoO_4)_2$ (Ln = Pr, Nd, Sm, Eu). *Proc. SPIE* **2013**, *8771*, 87711A−87711A-9.

(19) Bhattacharya, A. K.; Mallick, K. K.; Hartridge, A. Phase transition in $BiVO_4$. *Mater. Lett.* **1997**, *30* (1), 7−13.

(20) Liu, J.; Wang, H.; Wang, S.; Yan, H. Hydrothermal preparation of $BiVO_4$ powders. *Mater. Sci. Eng., B* **2003**, *104* (1−2), 36−39.

(21) Bierlein, J. D.; Sleight, A. W. Ferroelasticity in $BiVO_4$. *Solid State Commun.* **1975**, *16* (1), 69−70.

(22) Sameera, S.; Prabhakar Rao, P.; James, V.; Divya, S.; Raj, A. K. V. Influence of $(LiLa)_{1/2}MoO_4$ substitution on the pigmentary properties of $BiVO_4$. *Dyes Pigm.* **2014**, *104* (0), 41−47.

(23) Standard tables for reference solar spectral irradiances: Direct normal and hemispherical on 37° tilted surface; ASTM International: West Conshohocken, PA, 2012.

(24) Butler, M. A. Photoelectrolysis and physical properties of the semiconducting electrode WO_2. *J. Appl. Phys.* **1977**, *48* (5), 1914−1920.

(25) Zhou, L.; Wang, W.; Liu, S.; Zhang, L.; Xu, H.; Zhu, W. A sonochemical route to visible-light-driven high-activity $BiVO_4$ photocatalyst. *J. Mol. Catal. A: Chem.* **2006**, *252* (1−2), 120−124.

(26) Prokofiev, A. V.; Shelykh, A. I.; Golubkov, A. V.; Smirnov, I. A. Crystal growth and optical properties of rare earth sesquiselenides and sesquisulphides—New magneto-optic materials. *J. Alloys Compd.* **1995**, *219* (1−2), 172−175.

(27) Zou, Z.; Ye, J.; Arakawa, H. Role of R in Bi_2RNbO_7 (R = Y, rare earth): Effect on band structure and photocatalytic properties. *J. Phys. Chem. B* **2001**, *106* (3), 517−520.

(28) Machida, M.; Yabunaka, J.-i.; Kijima, T. Efficient photocatalytic decomposition of water with the novel layered tantalate $RbNdTa_2O_7$. *Chem. Commun.* **1999**, No. 19, 1939−1940.

(29) Panchal, V.; Errandonea, D.; Segura, A.; Rodríguez-Hernandez, P.; Muñoz, A.; Lopez-Moreno, S.; Bettinelli, M. The electronic structure of zircon-type orthovanadates: Effects of high-pressure and cation substitution. *J. Appl. Phys.* **2011**, *110* (4), 043723.

(30) Radhika, S. P.; Sreeram, K. J.; Unni Nair, B. Mo-Doped cerium gadolinium oxide as environmentally sustainable yellow pigments. *ACS Sustainable Chem. Eng.* **2014**, *2* (5), 1251−1256.

DOI: 10.1021/acssuschemeng.5b00198
ACS Sustainable Chem. Eng. 2015, 3, 1227−1233